**Geomechanics and Engineering**, *Vol. 19, No. 6 (2019) 523-532*
DOI: https://doi.org/10.12989/gae.2019.19.6.523


# Temperature distribution during heavy oil thermal recovery considering the effect of insulated tubing

Songting Zhang*

*Research Institute of Petroleum Engineering Technology, Shengli oilfield, SINOPEC, Xisan Road No. 306, Dongying 257000, Shandong, People's Republic of China*

*(Received June 6, 2019, Revised December 5, 2019, Accepted December 6, 2019)*

**Abstract.** Based on the formation characteristics, wellbore parameters and insulated tubing (IT) parameters of the Shengli oilfield, Shandong, China, a geomechanical model is built to predict the temperature distributions of the wellbore and formation. The effects of the IT heat conductivity coefficient (HCC), well depth and IT joint on the temperature distribution of the IT, completion casing, cement sheath, and formation are investigated. Results show the temperature of the formation around the wellbore has an exponentially decreasing relation with the distance to the wellbore. The temperature of the formation around the wellbore has an inverse relation with the IT HCC when the temperatures of the steam and the formation are given. The temperature of the casing outer wall is mainly determined by the steam temperature and IT HCC rather than by the initial formation temperature. The temperature of the casing at the IT joint is much larger than that of the other location. Due to the IT joint having a small size, the effects of the IT joint on the casing temperature distribution are limited to a small area only.

**Keywords:** energy geomechnics; heavy oil reservoir; thermal recovery; temperature; insulated tubing; heat conductivity coefficient; completion casing

## 1. Introduction

China has abundant heavy oil resources. The cumulative exploration reserves reached about 1.6 billion tons at the end of 2017. They are located mainly in the Liaohe oilfield, the Shengli oilfield, the Henan oilfield and the Xinjiang oilfield (Duan *et al.* 2019, Cao *et al.* 2012, Xi *et al.* 2013). The heavy oil has large viscosity, high starting pressure, and strong sensitivity to the temperature. Thermal recovery is one of the most effective methods to exploit the heavy oil (Liu *et al.* 2019, Huang *et al.* 2018, Pang *et al.* 2018). The commonly-used exploitation methods in China for the heavy oil include steam huff and puff and steam drive. Usually, the steam huff and puff is used first until the exploitation reaches a certain degree, and then the steam drive is used to improve the production and recovery efficiency (Dong *et al.*, 2019). Fig. 1 presents schematic diagrams of the steam huff and puff for heavy oil recovery. The steam huff and puff for heavy oil recovery includes three sub-steps (Jha *et al.* 2013, Al-Murayri *et al.* 2016).

(1) Huff (Fig. 1(a))

High temperature and high pressure (HTHP) steam is injected into the heavy oil reservoir. The amount of the steam injected usually is more than a thousand tons. The injecting time usually ranges from several days to more than ten days.

(2) Shut-in for soaking

When the stream injection is completed, the well is shut-in to allow soaking. During the soaking, the heat carried by the steam is exchanged with the reservoir sufficiently and effectively, and the heavy oils are heated. The time for the soaking usually is two to five days.

(3) Puff (Fig. 1(b))

The puff usually includes the stages blowing and pumping. The blowing usually lasts for several days, and the production liquids are mainly composed of the condensate water and hot oil. The injection of the HTHP steam increases the reservoir pressure in the zone around the bottomhole, which provides the energy for the blowing. When the flowing bottomhole pressure is equal to or is smaller than the blowing pressure, the pumping is started. The pumping usually lasts for several months to one year, and is the main production period of the oil. When the pumping production reaches the economical limit, a new steam huff and puff is carried out. Due to the pre-heating and plugging removal of the first steam huff and puff, the peak production of the second cycle is usually larger than that of the first cycle. However, the peak production decreases gradually beyond the third cycle. The above cycles is repeated until there are no economic benefits. The steam huff and puff is completed, and the stream drive (Dong *et al.* 2019) and other recovery techniques (Amirian *et al.* 2018) can be considered in the later exploitation.

The HTHP steam is injected into the reservoir through the wellbore during the heavy oil thermal recovery. The thermal conduction in the formation is a complicated process. How to accurately predict the temperature distribution and heat transfer efficiency is a hot topic in this field. Many researchers have done many constructive works on this topic, and numerous achievements have been obtained. Emami-Meybodi *et al.* (2014) developed a two-

*Corresponding author, Professor
E-mail: zhangst_sinopec@163.com



ISSN: 2005-307X (Print), 2092-6219 (Online)

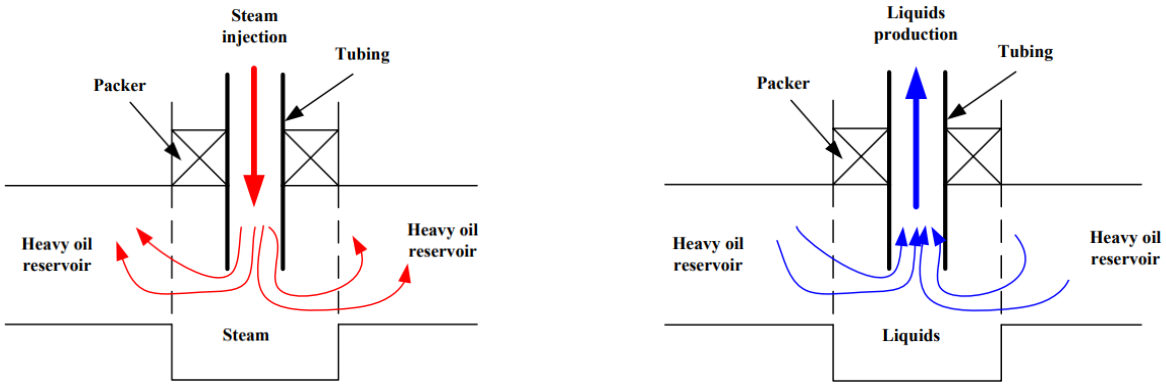


(a) Huff (b) Puff

Fig. 1 Schematic diagram of steam huff and puff for heavy oil recovery

dimensional transient heat conduction model to predict heat transfer from a horizontal wellbore to the formation during a steam circulation process. Dong *et al.* (2015) proposed a new method to increase the heavy oil reservoir recovery efficiency based on a multi-thermal fluid injection technology and steam assisted gravity drainage theory, and investigated the temperature distribution of the reservoirs. Gu *et al.* (2015) established a mathematical model to calculate the heat transfer efficiency of the wellbore during heavy oil thermal recovery, and analyzed the mechanism of the steam huff and puff improving the recovery efficiency. Amirian *et al.* (2015) employed an artificial neural network to predict the steam assisted gravity drainage production in heterogeneous reservoirs. They concluded that artificial neural networks have a good applicability to investigate heavy oil thermal recovery. Hassanzadeh *et al.* (2016 a, b, 2017) analyzed the conductive heat transfer during in-situ electrical heating of oil sands, and gave some constructive suggestions. Akhmedzhanov *et al.* (2016) discussed the heat transfer rate of using the sinusoidal like wells for heavy oil thermal recovery, and indicated providing constant hot water, steam, and electrical power supply by solar energy could reduce the costs. Siavashi and Doranehgard (2017) used a particle swarm optimization approach to build a mathematical model to optimize the hot water injection in heavy oilfields, and investigated the effects of the hot water temperature, injection rate and flowing bottomhole pressure on single well production. Sun *et al.* (2017) proposed a model to predict the thermo-physical properties of superheated steam in injection wells and to estimate wellbore heat transfer efficiency. Huang *et al.* (2018) developed an instrument to simulate heavy oil recovery using hot water, steam, or a multi-thermal fluid, and analyzed their mechanisms improving the well production. Saripalli *et al.* (2018) developed a new semi-analytical model to predict heavy oil production using cyclic steam stimulation in horizontal wells and validated by numerical simulations. Wang *et al.* (2018) studied the effects of CO2 on the recovery efficiency of steam assisted gravity drainage and proved that the temperature was the key factor determining the CO2 solubility in heavy oil. Moradi *et al.* (2018) studied the wellbore stability under HTHP and indicated the HTHP has decisive effects on the rock mechanical properties. Al-Gawfi *et al.* (2019) studied the interphase mass transfer problem using solvent aided thermal recovery theory, and concluded that the temperature and pressure were the key factors affecting the heavy oil thermal recovery efficiency. Dong *et al.* (2019) described some methods to enhance oil recovery for heavy oil and oilsands reservoirs after steam injection. They stated that decreasing the energy consumption and increasing the single well production were critical issues. Wu *et al.* (2019) built a two-dimensional visualization instrument to quantitatively investigate the sweep efficiency of steam and mixtures of steam and air, and pointed that the mixture of steam and air was better than the steam in improving the sweep efficiency. From the above literature review, we can conclude that: (1) the thermal recovery is the most effective method for heavy oil exploitation, but many challenges and difficulties still exist and are widely of concern; (2) accurately predicting the temperature distribution, heat transfer efficiency and thermal fluid seepage are the problems that should be urgently resolved.

To ensure the steam quality at the well bottom and to improve the thermal recovery efficiency, the heat loss along the wellbore has to be controlled strictly during the steam injection. The HTHP steam is usually transferred by the IT into the reservoir to reduce the heat loss and any completion casing damage. The parameters of the IT directly determine the temperature distribution of the wellbore and in the formation around the wellbore. The aim of this paper is to investigate the effects of the IT parameters on the temperature distribution of the wellbore and in the formation around the wellbore during heavy oil thermal recovery. First, a geomechanical model is built based on the formation features, the wellbore size and the IT size of the Shengli oilfield to predict the temperature distribution during the thermal recovery. Second, the effects of the IT heat conductivity coefficient (HCC) and IT joint on the temperatures of formation, casing, and wellbore are investigated using the proposed model. Third, some conclusions for deeper understanding of the temperature distribution considering the influence of the IT are given. Suggestions for the IT selection are also proposed. This study can deepen the understanding of the formation temperature distribution during heavy oil thermal recovery, and provides a base for the IT selection in the Shengli oilfield.

## 2. Numerical model and boundary conditions

### *2.1 Structure and controlling parameters of the insulated tubing*

To improve the thermal recovery efficiency, supercritical steam is used for the heavy oil exploitation. The temperature and pressure of the supercritical steam can reach about 373 ℃ and 22 MPa respectively (Oxana *et al.*, 2019). If such HTHP steam is injected directly through the wellbore into the reservoir, two adverse consequences will happen. (1) Thermal damage of the completion casing takes place. The HTHP steam produces high stress in the casing, which may exceed the yield stress of the casing. Moreover, the casing strength will decrease greatly as a result of the high temperature (Zhu *et al.*, 2013). These two factors notably increase the potential for a casing failure. (2) Large heat losses in the overlying formation. The completion casing has a good capacity for transferring heat. A lot of heat is lost into the formation when the HTHP steam passes through the casing. This heat loss decreases the heat usage efficiency. Therefore, the IT is used for the steam injection. It is located in the completion casing and hangs from the wellhead. Fig. 2 presents the structure of the wellbore used for the heavy oil thermal recovery in the Shengli oilfield. The wellbore includes the insulated tubing, completion casing, and cement sheath. The IT passes through the completion casing. The annulus between the IT and the casing is full filled nitrogen. The casing is cemented firmly with the formation. There are perforations in the casing and in the cement sheath at the intersection with the oil reservoir, which are the paths for the steam and oil flow. The IT has a double-layer structure. To increase the capacity of the thermal insulation, the IT annulus between the two layers is filled with high insulation material (e.g., aerogel). The length of the wellbore in the Shengli oilfield is about 1200 m. The single IT is connected by the joints to form a steam channel. The joints are made from steel, which has good heat conductivity. The HCC is the key factor in determining the heat-conducting property of the IT. It is defined as the heat transfer through a unit area in one second when the temperature difference between the inner and outer walls of the tubing is 1° K and the length of the tubing is 1 m. Its unit is W/(m·K) (Kim *et al.* 2019, Teltayev *et al.* 2015). An IT with a high HCC indicates a poor insulation performance and more heat loss through the IT during the thermal recovery. By adjusting the property of the insulation material filling the IT annulus, the HCC of the IT can be controlled accurately. The IT size of the Shengli oilfield has an inner diameter of 62 mm, an outer diameter of 111.3 mm, and the thickness of its annulus of 21.39 mm. The IT HCCs are 0.001 W/(m·K), 0.006 W/(m·K), 0.01 W/(m·K), 0.06 W/(m·K) and 0.12 W/(m·K), which can be selected based on the field requirement. Due to the main objection of the paper is to investigate the effects of insulated tubing parameters on the formation temperature, the effects of coke formation and gas generation on the heat transfer (Hassanzadeh, 2016 a, b) are not included.

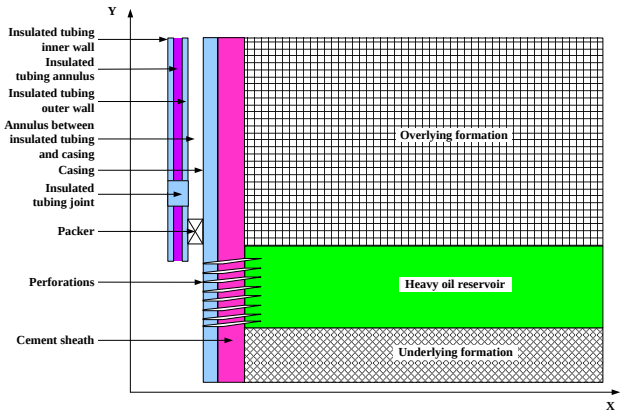


Fig. 2 Structure of the wellbore used for the heavy oil thermal recovery of Shengli oilfield

### *2.2 Numerical model and boundary conditions*

To study the effect of the IT on the temperature distribution around the wellbore during the thermal recovery, a geomechanical model is built. Fig. 3 presents the model used for the temperature calculation of the heavy oil thermal recovery and its boundary conditions when the effects of the insulated tubing are considered. To show the detailed dimensions, an enlarged view of the insulated tubing joint is also included in the figure. The model is built using ANSYS (ANSYS Inc, 2012). It is a rectangle with a height of 70 m and a length of 1000 m. The heights of the heavy oil reservoir, overlying formation and underlying formation are 10 m, 40 m and 20 m respectively. The vertical central axis of the wellbore is the left boundary of the model. The temperature of the location with a distance of 1000 m to the wellbore axis is assumed to be not affected by the steam temperature, viz., remains equal to the initial temperature of the formation. During the thermal recovery, the prediction of the temperature distribution along the vertical direction of the formation can be simplified as a plane axisymmetric problem. Considering the symmetry, a 1/2 geomechanical model is established to improve the calculating efficiency. When constructing the model, we assume that the cementing is in good condition, and that there is no slippage among the interfaces between casing and cement sheath, and cement sheath and formation. From the left to the right, we see in turn the IT inner wall, IT annulus, IT outer wall, IT-Casing annulus, casing, cement sheath, and the formation. The inner diameter of the IT is 62 mm, the thicknesses of the inner and outer wall of the IT are 6.35 mm, and the thickness of the IT annulus is 13.45 mm. The outer diameter of the casing is 177.8 mm, and the casing wall thickness is 10.36 mm. The cement sheath has a thickness of 30 mm in all directions, and is assumed to be perfect (Yan *et al.*, 2017; Zhu *et al.*, 2016). The reservoir beyond the outside of the cement sheath has a length of about 1000 m. To investigate the effects of the IT on the temperature distribution of the formation and casing, different HCCs of the IT are simulated. During calculating the temperature distribution around the wellbore along the entire well depth, the effects of the IT joints are not included. The entire tubing string is assumed as a uniform

Table 1 Material properties used in the numerical simulations

| Materials Items | IT | IT annulus | Casing-IT annulus (nitrogen) | Casing | Cement sheath | Formations |
|---|---|---|---|---|---|---|
| Density (Kg/m$^3$) | 7850 | 150 | 0.881 | 7850 | 1830 | 2720 |
| HCC W/(m·K) | 43.27 | 0.001~0.12 | 0.024 | 43.27 | 0.81 | 3.44 |
| Specific heat (J/kg.K) | 468.92 | 669.89 | 1050.9 | 468.92 | 879.23 | 866.67 |
| Young's modulus (GPa) | 118 | | | 194 | 15~28 | 14~20 |
| Poisson's ratio | 0.26 | | | 0.26 | 0.12~0.17 | 0.18~0.22 |
| Coefficient of thermal expansion ($10^{-6}$℃) | 12 | | | 11.7 | 10.3 | 10.3 |

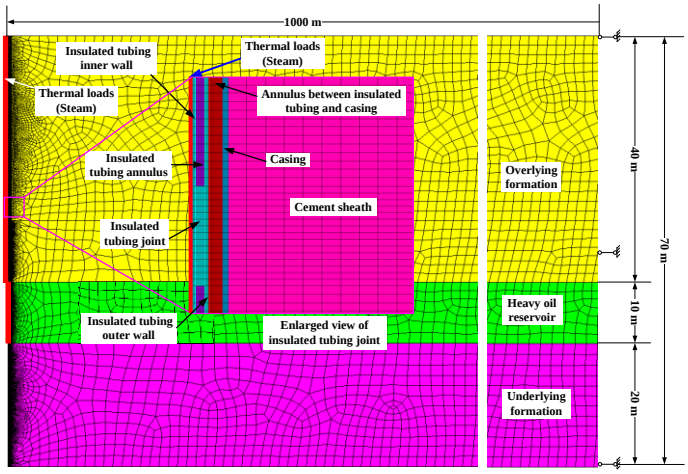


Fig. 3 Geomechanical model for the temperature calculation of the heavy oil thermal recovery and its boundary conditions when the effects of the insulated tubing are considered. To show the detailed dimensions, an enlarged view of insulated tubing joint is also included in the figure

structure. The other boundary conditions are the same as those in Fig. 3.

The thermal loads apply to the IT inner wall and the left boundary of the heavy oil reservoir. The steam temperature is 373°C. The formation temperature is applied uniformly to the model as the intimal condition. Based on the data of the given area of the Shengli oilfield, the temperature of the formation at a depth of 1200 m is about 68°C. The formation temperature gradient is about 4°C /100 m. The model right boundary is maintained at a constant temperature of 68°C. The material properties used in the numerical simulations are given in Table 1. Considering that the steam injection is usually completed in two weeks, the calculating time is set as 14 days. The formation temperature has a linear relation with depth. Different initial formation temperatures viz., 20°C (0 m), 36°C (400 m), 52°C (800 m), 68°C (1200 m) are simulated to represent the formation depths. The IT HCCs are simulated as 0.001 W/(m·K), 0.006 W/(m·K), 0.0086 W/(m·K), 0.01 W/(m·K), 0.06 W/(m·K) and 0.12 W/(m·K) respectively.

To eliminate the boundary effects on the results, the model has large dimensions. However, the dimensions of the IT, casing, and cement sheath are small, in the millimeter level, much smaller than those of the formations (70 m ×1000 m). Moreover, we only are interested in the results in the zones immediately around the wellbore. During meshing the model, the meshes with a small uniform size are used for the IT inner wall, IT annulus, IT outer wall, IT-Casing annulus, casing, and cement sheath to ensure the calculating accuracy. Radial grids are used to mesh the overlying and underlying formations as well as the reservoir. The elements near the wellbore are small, and the element size increases with increasing distance to the wellbore. Axisymmetric quadrilateral thermal solid elements are used. The model contains 30474 elements and 30475 nodes. To avoid poor mesh quality, the Meshtool embedded in ANSYS software is used to check the mesh quality before simulations. To ensure the numerical results are independent from the element size, elements with different sizes have been tried to find the best size. The results show that the element type, size and boundary conditions used in the model satisfy the calculating accuracy and convergence requirements.

## 3. Results and affecting factor analysis

### *3.1 Influence of the heat conductivity coefficient on the formation temperature distribution*

To investigate the effects of the IT HCC on the temperature distribution in the formations, the IT HCCs are simulated as 0.001 W/(m·K), 0.006 W/(m·K), 0.01 W/(m·K), 0.06 W/(m·K) and 0.12 W/(m·K). Fig. 4 presents the temperature contours of the formation for different IT HCC values when the steam temperature is 373°C, injection

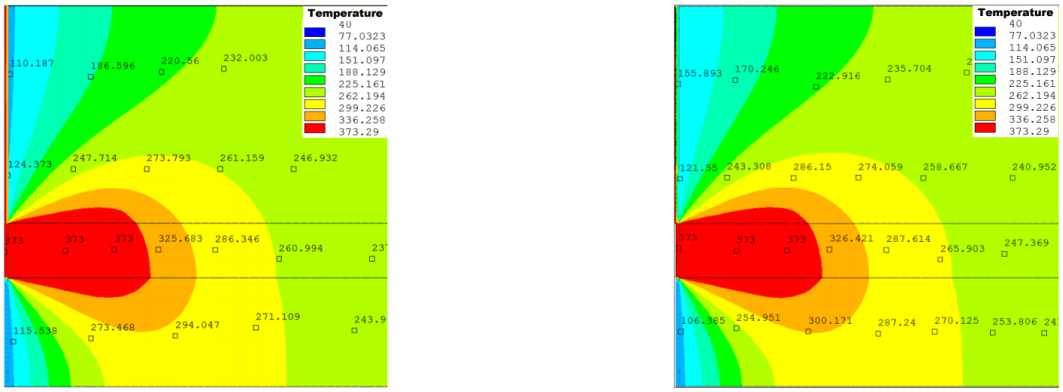


(a) 0.12 W/(m·K) (b) 0.006 W/(m·K)

Fig. 4 Temperature contours in the formation under different IT heat conductivity coefficients when the steam temperature is 373°C, injecting time is 14 days, and the initial temperature of the formation is 68°C

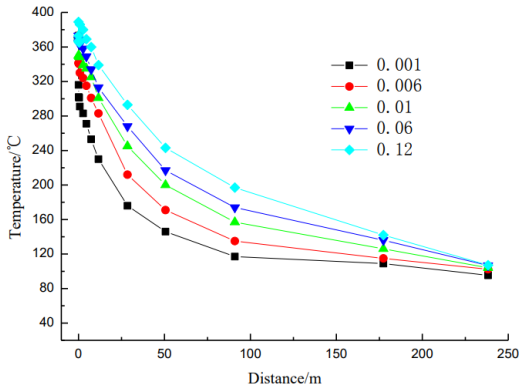


Fig. 5 Relations between the temperature and the distance to the wellbore for five different IT heat conductivity coefficients when the steam temperature is 373°C, injecting time is 14 days, and the initial temperature of the formation is 68°C

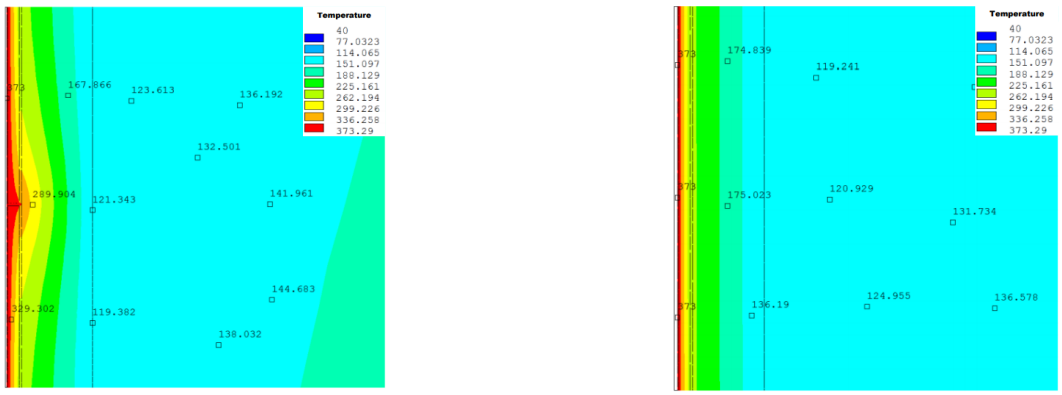


(a) With the joint (b) Without the joint

Fig. 6 Temperature contours of the wellbore without and with the effects of the IT joint when the steam temperature is 373°C, injecting time is 14 days, the initial temperature of the formation is 68°C, and the IT heat conductivity coefficient is 0.006 W/(m·K)

time is 14 days, and the initial temperature of the formation is 68°C. When the IT has a large HCC (Fig. 4(a)), a large area of high temperature (red zone) is produced around the wellbore. The area of the red zone around the wellbore (Fig. 4(b)) decreases greatly when the IT has a small HCC. This is mainly because the heat carried by the steam is lost continuously into the formation around the wellbore when the IT has a large HCC, and thereby heats the overlying formation. When the IT has a small HCC, only a small amount of heat can transfer into the formation through the wellbore. Most of the heat carried by the steam is transferred into the reservoir. The results have good accordance with available related results (Emami-Meybodi *et al.* 2014, 2016 a, b, 2017).

By comparing the temperature of the reservoir, it is seen that the IT HCC has little effect on the reservoir

temperature distribution. This indicates that the heat transferred into the reservoir by the two ITs is large enough to form steady high temperature zones, and that the heat lost through the IT with large HCC accounts for only a small portion of the total heat carried by the steam. The results also indicate that there is a potential for reducing the steam injection time of 14 days.

Fig. 5 presents the relations between the temperature and the distance to the wellbore for five different IT HCCs when the steam temperature is 373°C, injecting time is 14 days, and the initial temperature of the formation is 68°C. The temperature decreases with the increase of the distance to the wellbore, and trends to equaling the initial temperature of the formation. The temperature in the zone directly around the wellbore is largely determined by the IT HCC, especially in the zone from the wellbore edge to 30 m away from the wellbore. The temperature in this zone decreases notably with a decrease of the IT HCC. For example, when the IT HCCs are 0.12 W/(m·K), 0.06 W/(m·K), 0.01 W/(m·K), 0.006 W/(m·K) and 0.001 W/(m·K), the temperatures of a point at 4.59 m from the wellbore are 369.81°C, 349.45°C, 335.87°C, 315.92°C and 271.41°C respectively. This confirms that there is more heat loss into the overlying formation and a decrease in the heat usage efficiency when the IT has a large HCC. Moreover, the lost heat may increase the casing stress and may decrease the casing strength, which increases the risk of casing failure. For an actual engineering application, an IT with an HCC smaller than 0.006 W/(m·K) is recommended. The results also show that the temperature in the zone around the wellbore has an exponential decrease relation with the distance to the wellbore. It indicates that the temperature change takes place only in a small zone near the wellbore, which is in accordance with published research (Gu *et al.* 2015, Miah *et al.* 2018). This proves that the model and its boundaries used for this paper are reliable and accurate

### *3.2 Influence of the depth on the formation temperature*

To study the effects of the depth on the induced temperature distribution, different depths are simulated by adjusting the initial temperature of the formation. Considering that the depth of the Shengli heavy oil reservoir is about 1200 m and that the length of the IT joint is only 0.2 m, the effects of the IT joint are not included in the simulation. The IT string is assumed as a continuous and uniform structure. To validate this assumption, the temperature distributions of the IT with and without the IT joints are determined. Fig. 6 presents the temperature contours of the wellbore without and with the effects of the IT joint when the steam temperature is 373°C, injecting time is 14 days, initial temperature of the formation is 68°C, and the IT HCC is 0.006 W/(m·K). By comparing the results in Fig. 6(a) with those in Fig. 6(b), it can be seen that the temperature of only a small zone around the IT joint is affected by the joints, due to its small size. This indicates that the assumption that the IT string is a continuous and uniform structure is reasonable for studying the effects of the depth on the temperature distribution.

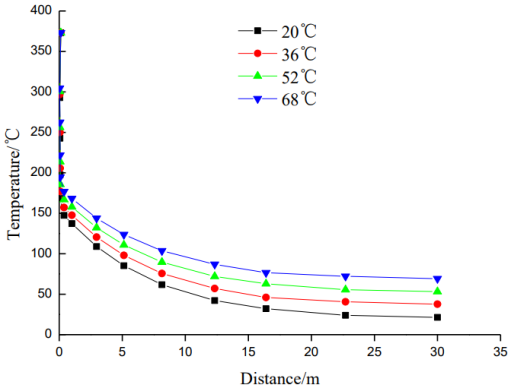


Fig. 7 Relations between the temperature and the distance to the wellbore for four different initial temperatures of the formation (corresponding to different depths) when the steam temperature is 373°C, injecting time is 14 days, and the IT heat conductivity coefficient is 0.006 W/(m·K)

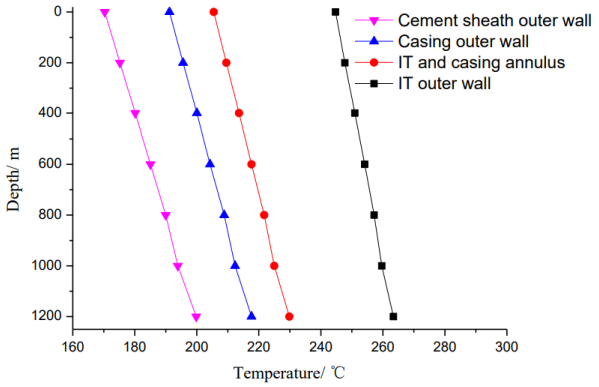


Fig. 8 Relations between the temperatures of the IT outer wall, IT and casing annulus, casing outer wall, and cement sheath outer wall and the depth when the steam temperature is 373°C, injecting time is 14 days, and the IT heat conductivity coefficient is 0.006 W/(m·K)

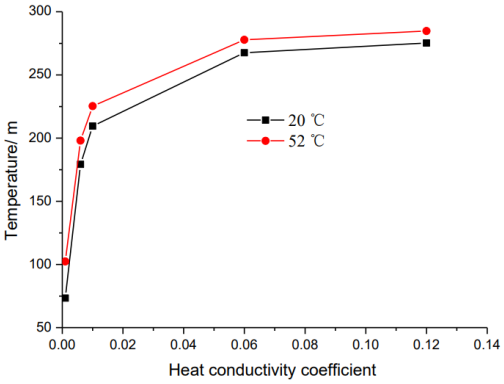


Fig. 9 Relations between the temperatures of the casing outer wall and IT heat conductivity coefficient for two different initial temperatures of the formation when the steam temperature is 373°C, and injecting time is 14 days

Fig. 7 presents the relations between the temperature and the distance to the wellbore for four different initial temperatures of the formation (corresponding to different depths) when the steam temperature is 373°C, injecting time is 14 days, and the IT HCC is 0.006 W/(m·K). The

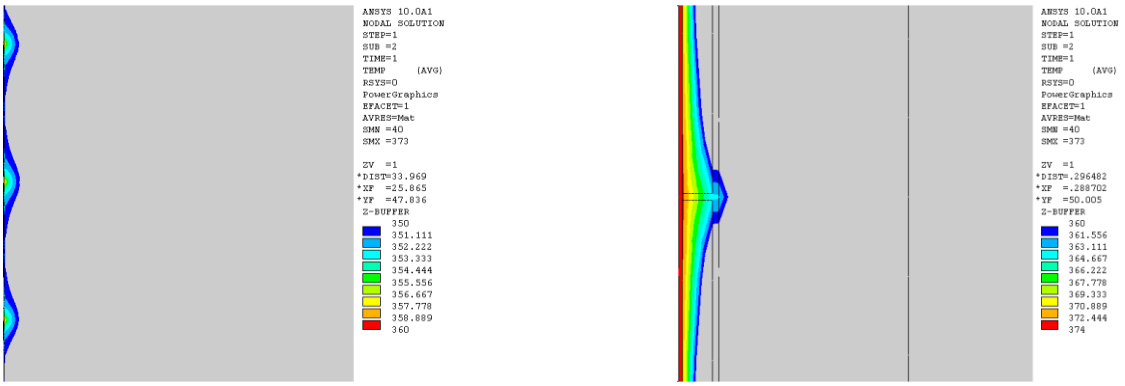


(a) Locations of the IT joints (b) Enlarged view near a single IT joint

Fig. 10 Temperature contours around the IT joint when the steam temperature is 373°C, injecting time is 14 days, initial temperature of the formation is 40°C, and the IT heat conductivity coefficient is 0.006 W/(m·K)

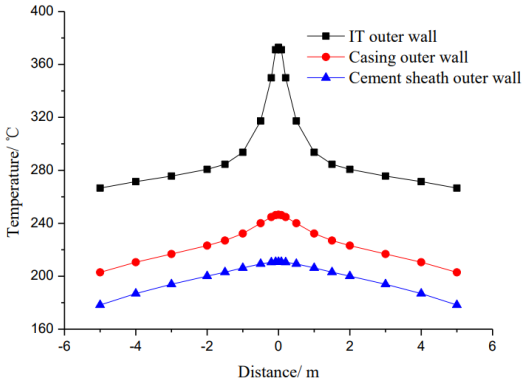


Fig. 11 Relations between the temperatures of IT outer wall, casing outer wall, and cement sheath outer wall at the locations of the IT joint and the distance from the middle point of the joint when the steam temperature is 373°C, injecting time is 14 days, the initial temperature of the formation is 40°C, and the IT heat conductivity coefficient is 0.006 W/(m·K)

temperature decreases, and its decrease rate is gradually reduced and trends to a stable value with increasing distance to the wellbore. The temperatures of the IT inner wall, IT outer wall, casing outer wall and cement sheath outer wall are included in Fig. 7, and they are mainly determined by the steam temperature rather than by the formation initial temperature. When the distance to the wellbore increases to more than 2 m, the effects of the formation initial temperature become notable. For example, the temperatures of the point at 2.97 m from the wellbore are 108.83°C, 120.52°C, 132.21°C and 143.91°C respectively when the initial temperatures of the formation are 20°C (0 m), 36°C (400 m), 52°C (800 m), 68°C (1200 m). The increase rate of the temperatures at this point is smaller than that of the formation initial temperature. It indicates that the temperature of the zone around the wellbore is mainly determined by the steam temperature and IT HCC rather than by the formation initial temperature.

Fig. 8 presents the relations between the temperatures of the IT outer wall, IT and casing annulus, casing outer wall, and cement sheath outer wall and the depth when the steam temperature is 373°C, injecting time is 14 days, and the IT HCC is 0.006 W/(m·K). The temperatures at all four locations increase with the depth, and show a linear relation with depth. The results also indicate that the temperatures of the IT outer wall, IT and casing annulus, casing outer wall, and cement sheath outer wall increase slightly with increasing depth. For example, the temperatures of the IT outer wall, IT and casing annulus, casing outer wall, and cement sheath outer wall are 247.75°C, 209.52°C, 195.58°C and 175.21°C at the depth of 200 m, and 263.40°C, 229.84°C, 217.64°C and 199.80°C at the depth of 1200 m, increments of about 6.32%, 9.67%, 11.28% and 14.03% respectively. It also indicates that the formation initial temperature is not the controlling factor for the temperature distribution of the zone around the wellbore. The results also show the effects of the depth on the temperature increase with increasing distance to the IT inner wall (steam). For example, the temperature of the IT outer wall at the depth of 1200 m increases by about 6.32% over that at the depth of 200 m. Under the same conditions, the temperature of the cement sheath outer wall increases about 14.03%. This indicates that the IT is the key factor affecting the temperature distribution of the wellbore, and its influence decreases with the increase of the distance from the well.

### *3.3 Influence of the heat conductivity coefficient on the casing temperature*

Fig. 9 presents the relations between the temperatures of

the casing outer wall and IT HCC under different initial temperatures of the formation when the steam temperature is 373°C, and injecting time is 14 days. The temperatures of the casing outer wall increase with an increase of the IT HCC. When the HCC is small, the casing outer wall temperature increases sharply with increasing HCC. For example, the casing outer wall temperature increases from 96.1°C to 185.82°C when the IT HCC increases from 0.001 W/(m·K) to 0.006 W/(m·K) under the formation initial temperature of 52°C. This is due to the fact that the heat transfer is determined by the HCC. A small HCC means less heat lost. When the HCC increases beyond a critical value, the heat transferred into the casing is balanced with the heat lost from the casing, and the casing temperature no longer increases. The results show that the critical value of the IT used in the Shengli oilfield is 0.02 W/(m·K). When the IT HCC is larger than 0.02 W/(m·K), the IT has little effect on decreasing the risk of casing damage, and lots of heat is lost. The results also show that the formation initial temperature has only slight effects on the casing outer wall temperature. The reason has been given in Section 3.2.

By using the data given in Fig. 9, the following equations between the casing outer wall temperature and the IT HCC under different formation initial temperatures are obtained:

(1) Formation initial temperature of 20°C:

$$T_{20} = 254.18 - 211.76e^{-139.90K_{xx}}$$

(2) Formation initial temperature of 52°C:

$$T_{52} = 263.46 - 191.23e^{-139.90K_{xx}}$$

where $T_{20}$ and $T_{52}$ are the temperatures of the casing outer wall when the formation initial temperatures are 20°C and 52°C respectively; $K_{xx}$ is the IT HCC.

The results show that the IT HCC is the key factor affecting the casing temperature. Decreasing the IT HCC can effectively prevent the failure of the casing taking place.

### *3.4 Influence of the insulated tubing joint on the temperature distribution*

Based on the results of Section 3.2, the IT joint has little effect on the temperature distribution along the entire wellbore but greatly affects the local temperature distribution. Fig. 10 presents the temperature contours around the IT joint when the steam temperature is 373℃, injecting time is 14 days, the initial temperature of the formation is 40°C, and the IT HCC is 0.006 W/(m·K). To show the temperature in the joint clearly, the temperature ranging from 350°C to 360°C is highlighted in Fig. 10 (a), and the temperature ranging from 360°C to 373°C is highlighted in Fig. 10 (b). The temperature in the zone around the IT joint is much higher than that of the other areas. This is mainly because the joint is made of steel, which has a large HCC, about 43.27 W/(m·K). A semicircular high temperature region forms at the joint. The results also show that the high temperature regions have only small areas

To quantitatively evaluate the effects of the IT joint on the temperature distribution of the zone around the joint, the temperatures of the IT outer wall, casing outer wall and cement sheath outer wall are monitored. Fig. 11 presents the relations between the temperatures of IT outer wall, casing outer wall, and cement sheath outer wall at the locations of the IT joint and the distance when the steam temperature is 373°C, injecting time is 14 days, the initial temperature of the formation is 40°C, and the IT HCC is 0.006 W/(m·K). In Fig. 11, the horizontal coordinate 0 represents the middle point of the joint, and the positive value indicates a position above the middle point, a negative value a position below the middle point. The temperatures at the middle point have the maximum, and they decrease towards the two ends, which show symmetry along the middle point of the joint. The temperature of the IT outer wall is the highest followed by that of the casing outer wall and the cement sheath outer wall. The temperature of the IT outer wall is much higher than that of the casing outer wall and the cement sheath wall. The temperature difference between the casing outer wall and the cement sheath wall is small. This is because the joint conducts the steam temperature directly, and the joint is good conductor of heat. This causes the temperature of the IT outer wall to be high, basically equal to the steam temperature. The IT-Casing annulus is full of nitrogen. The HCC of nitrogen is about 0.024 W/(m·K), much smaller than that of the joint. This results in the temperature of the casing outer wall to be much lower than that of the IT outer wall. The cement sheath has a HCC of 0.81 W/(m·K) and a thickness of 30 mm, which causes the temperature difference between the casing outer wall and cement sheath wall to be small. The results also show that the IT outer wall temperature is affected mostly by the joint, followed by the casing outer wall and the cement sheath outer wall. For example, the temperatures of the IT outer wall, casing outer wall and cement sheath outer wall are 266.57°C, 202.94°C and 178.26°C at the 5 m point while they are 372.90°C, 246.48°C and 210.82°C at the middle point, increases of 39.89%, 21.45% and 18.27% respectively. This also shows that thermal expansion damage of the casing and the cement sheath more easily takes place at the IT joints than at the other locations.

## 4. Conclusions

(1) Based on the parameters of the insulated tubing, completion casing, cement sheath and formation used for the heavy oil thermal recovery of the Shengli oilfield, a geomechanical model is proposed to determine the temperature distribution around the wellbore. The effects of the insulated tubing heat conductivity coefficient, formation depth and insulated tubing joint on the temperature distributions of the insulated tubing, casing, cement sheath and formation are investigated.

(2) When the insulated tubing has a small heat conductivity coefficient, the temperature of the formation has an exponential decrease with increasing distance to the wellbore. Only small zones around the wellbore change their temperature greatly during the thermal recovery, which has a good accordance with published research. This indicates that the model and boundary conditions proposed

in the paper are reliable.

(3) The temperature of the zone around the wellbore is proportional to the heat conductivity coefficient of the insulated tubing when the steam temperature and formation initial temperature are given. Smaller heat conductivity coefficient of the insulated tubing means less heat loss, high heat usage efficiency and less risk of casing damage. The temperature of the casing is mainly determined by the stream temperature and the insulated tubing heat conductivity coefficient rather than by the formation temperature.

(4) The temperatures of the zone around the insulated tubing joint are much higher than those of other locations due to the high heat conductivity coefficient of the joint. However, the influence of the joint is constrained to only a small area because the joint has small dimensions.

## References


Akhmedzhanov, T., Nuranbayeva, B., Gussenov, I. and Ismagilova, L. (2017), "Enhanced oil recovery and natural bitumen production through the use of sinusoidal wells and solar thermal method", *J. Petrol. Sci. Eng.*, **159**, 506-512. https://doi.org/10.1016/j.petrol.2017.09.037.

Al-Gawfi, A., Nourozieh, H., Ranjbar, E., Hassanzadeh, H. and Abedi, J. (2019), "Mechanistic modelling of non-equilibrium interphase mass transfer during solvent-aided thermal recovery processes of bitumen and heavy oil", *Fuel*, **241**, 813-825. https://doi.org/10.1016/j.fuel.2018.12.018.

Al-Murayri, M., Maini, B., Harding, T. and Oskouei, J. (2016), "Multicomponent solvent Co-injection with steam in heavy and extra-heavy oil reservoirs", *Energy Fuel*, **30**(4), 2604-2616. https://doi.org/10.1021/acs.energyfuels. 5b02774.

Amirian, E., Dejam, M. and Chen, Z.X. (2018), "Performance forecasting for polymer flooding in heavy oil reservoirs", *Fuel*, **216**, 83-100. https://doi.org/10.1016/j.fuel.2017.11.110.

Amirian, E., Leung, J.Y., Zanon, S. and Dzurman, P. (2015), "Integrated cluster analysis and artificial neural network modeling for steam-assisted gravity drainage performance prediction in heterogeneous reservoirs", *Expert Syst. Appl.*, **42**(2), 723-740. http://dx.doi.org/10.1016/j.eswa.2014.08.034.

ANSYS, Inc., (2012), *ANSYS 14.5 Mechanical APDL Verification Manual*, Canonsburg, Pennsylvania, U.S.A. http://www.ansys.com.

Cao, Y., Liu, D., Zhang, Z., Wang, S., Wang, Q. and Xia, D. (2012), "Steam channeling control in the steam flooding of super heavy oil reservoirs, Shengli oilfield", *Petrol. Explor. Dev.*, **39**(6), 785-790. http://dx.doi.org/10.1016/s1876-3804(12)60105-0.

Dong, X., Liu, H., Chen, Z., Wu, K., Lu, N. and Zhang, Q. (2019), "Enhanced oil recovery techniques for heavy oil and oilsands reservoirs after steam injection", *Appl. Energy*, **239**, 1190-1211. https://doi.org/10.1016/j.apenergy. 2019.01.244.

Dong, X., Liu, H., Hou, J., Zhang, Z. and Chen, Z. (2015), "Multi-thermal fluid assisted gravity drainage process: a new improved-oil-recovery technique for thick heavy oil reservoir", *J. Petrol. Sci. Eng.*, **133**, 1-11. http://dx.doi.org/10.1016/j.petrol.2015.05.001.

Duan, M., Li, C., Wang, X., Fang, S., Xiong Y. and Shi, P. (2019), "Solid separation from the heavy oil sludge produced from Liaohe oilfield", *J. Petrol. Sci. Eng.*, **172**, 1112-1119. https://doi.org/10.1016/j.petrol.2018.09. 019.

Emami-Meybodi, H., Saripalli, H. and Hassanzadeh, H. (2014), "Formation heating by steam circulation in a horizontal wellbore", *Int. J. Heat Mass Tran.*, **78**, 986-992. http://dx.doi.org/10.1016/j.ijheatmasstransfer. 2014.07.063.

Gu, H., Cheng, L., Huang, S., Li, B., Shen, F., Fang, W. and Hu, C. (2015), "Steam injection for heavy oil recovery: modeling of wellbore heat efficiency and analysis of steam injection performance", *Energy Convers. Manage.*, **97**, 166-177. http://dx.doi.org/10.1016/j.enconman.2015.03.057.

Hassanzadeh, H. and Harding, T. (2016b), "Analysis of conductive heat transfer during in-situ electrical heating of oil sands", *Fuel*, **178**, 290-299. https://doi.org/10.1016/j.fuel.2016.03.070.

Hassanzadeh, H., Harding, T., Moore, R., Mehta, S. and Ursenbach, M. (2016a), "Gas generation during electrical heating of oil sands", *Energy Fuel.*, **30**(9), 7001-7013. https://doi.org/10.1021/acs.energyfuels.6b01227.

Hassanzadeh, H., Rabiei Faradonbeh, M. and Harding, T. (2017), "Numerical simulation of solvent and water assisted electrical heating of oil sands including aquathermolysis and thermal cracking reactions", *AIChE J.*, **63**(9), 4243-4258. https://doi.org/10.1002/aic.15774.

Huang, S., Cao, M. and Cheng, L. (2018), "Experimental study on the mechanism of enhanced oil recovery by multi-thermal fluid in offshore heavy oil", *Int. J. Heat Mass Transf.*, **122**, 1074-1084. https://doi.org/10.1016/j.ijheatmasstransfer.2018.02.049.

Jha, R., Kumar, M., Benson, I. and Hanzlik, E. (2013), "New insights into steam/solvent-coinjection process mechanism", *SPE J.*, **18**(5), 867-877. https://doi.org/10.2118/159277-PA.

Kim, S., Tserengombo, B., Choi, S., Noh, J., Choi, S., Chung, H., Kim, J. and Jeong, H. (2019), "Experimental investigation of heat transfer coefficient with Al2O3 nanofluid in small diameter tubes", *Appl. Therm. Eng.*, **146**, 346-355. https://doi.org/10.1016/j.applthermaleng.2018.10.001.

Liu, Y., Liu, X., Hou, J., Li, H., Liu, Y. and Chen, Z. (2019), "Technical and economic feasibility of a novel heavy oil recovery method: geothermal energy assisted heavy oil recovery", *Energy*, 853-867. https://doi.org/10.1016/j.energy. 2019.05.207.

Moradi, S., Nikolaev, N., Chudinova, I. and Martel, A. (2018), "Geomechanical study of well stability in high-pressure, high-temperature conditions", *Geomech. Eng.*, **16**(3), 331-339. https://doi.org/10.12989/gae.2018.16.3.331.

Oxana, N., Anatoly, A., Andrey, V. and Mikhail, Y. (2019), "Transformation of lignin under uniform heating. I. Gasification in a flow of water vapor and supercritical water", *J. Supercrit. Fluid*, **148**, 84-92. https://doi.org/10.1016/j.supflu.2019.03.001.

Pang, Z., Lyu, X., Zhang, F., Wu, T., Gao, Z., Geng, Z. and Luo, C. (2018), "The macroscopic and microscopic analysis on the performance of steam foams during thermal recovery in heavy oil reservoirs", *Fuel*, **233**, 166-176. https://doi.org/10.1016/j.fuel.2018.06.048.

Saripalli, H., Salari, H., Saeedi, M. and Hassanzadeh, H. (2018), "Analytical modelling of cyclic steam stimulation (css) process with a horizontal well configuration", *Can. J. Chem. Eng.*, **96** (2), 573-589. https://doi.org/ 10.1002/cjce.22958.

Siavashi, M. and Doranehgard, M. (2017), "Particle swarm optimization of thermal enhanced oil recovery from oilfields with temperature control", *Appl. Therm. Eng.*, **123**, 658-669. http://dx.doi.org/10.1016/ j.applthermaleng.2017.05.109.

Sun, F., Yao, Y., Chen, M., Li, X., Zhao, L. and Meng, Y. (2017), "Performance analysis of superheated steam injection for heavy oil recovery and modeling of wellbore heat efficiency", *Energy*, **125**, 795-804. http://dx.doi.org/10.1016/j.energy.2017.02.114.

Teltayev, B.B. and Aitbayev, K. (2015), "Modeling of transient temperature distribution in multilayer asphalt pavement", *Geomech. Eng.*, **8**(2), 133-152. http://dx.doi.org/10.12989/gae.2015.8.2.133.

Wang, C., Liu, P., Wang, F., Atadurdyyev, B. and Ovluyagulyyev, M. (2018), "Experimental study on effects of CO2 and

improving oil recovery for CO2 assisted SAGD in super-heavy-oil reservoirs", *J. Petrol. Sci. Eng.*, **165**, 1073-1080. https://doi.org/10.1016/j.petrol.2018.02.058.

Wu, Z., Wang, L., Xie, C. and Yang, W. (2019), "Experimental investigation on improved heavy oil recovery by air assisted steam injection with 2D visualized models", *Fuel*, **252**, 109-115. https://doi.org/10.1016/j.fuel.2019.04.097.

Xi, C., Guan, W., Jiang, Y., Liang, J., Zhou, Y. and Wu, J. (2013), "Numerical simulation of fire flooding for heavy oil reservoirs after steam injection: a case study on block H1 of Xinjiang oilfield, NW China", *Petrol. Explor. Dev.*, **40**(6), 766-773. https://doi.org/10.1016/S1876-3804(13)60102-0.

Yan, C., Deng, J., Cheng, Y. and Deng, F. (2017), "Rock mechanics and wellbore stability in Dongfang 1-1 Gas Field in South China Sea", *Geomech. Eng.*, **12**(3), 465-481. https://doi.org/10.12989/gae.2017.12.3.465.

Zhu, X., Liu, S. and Tong, H. (2013), "Plastic limit analysis of defective casing for thermal recovery wells", *Eng. Fail. Anal.*, **27**, 340-349. https://doi.org/10.1016/j.engfailanal.2012.07.011.

Zhu, X., Liu, W. and Zheng, H. (2016), "A fully coupled thermo-poroelastoplasticity analysis of wellbore stability", *Geomech. Eng.*, **10**(4), 437-454. https://doi.org/10.12989/gae.2016.10.4.437.

*CC*